Conformal SnO$_x$ Heterojunction Coatings for Stabilized Photoelectrochemical Water Oxidation using Arrays of Silicon Microcones

Ivan A. Moreno-Hernandez[1], Sisir Yalamanchili[3], Harold J. Fu[1], Harry A. Atwater[3,4], Bruce S. Brunschwig[2], Nathan S. Lewis[1,2,4]

[1]Division of Chemistry and Chemical Engineering, 127-72, California Institute of Technology, Pasadena, CA 91125, USA

[2]Beckman Institute Molecular Materials Research Center, California Institute of Technology, Pasadena, CA 91125, USA

[3]Division of Engineering and Applied Sciences, California Institute of Technology, Pasadena, CA 91125

[4]Kavli Nanoscience Institute, California Institute of Technology, Pasadena, CA 91125, USA

*Correspondence to: nslewis@caltech.edu

Supplementary Material

Materials and Methods

Materials Characterization

X-ray diffraction (XRD) analysis was performed with a Bruker D8 Discover instrument equipped with a Vantec-500 2-dimensional detector. Cu Kα radiation (1.54 Å) was generated at a tube current of 1000 μA and a tube voltage of 50 kV. The incident radiation was focused with a 0.5 mm diameter mono-capillary collimator. The samples were placed at the correct position for diffraction measurements by adjusting the sample position until the diffuse reflectance of an aligned laser beam was in the correct position. Measurements were collected with a coupled theta/2theta mode. The scattered radiation was collected with a Vantec-500 detector with an angular resolution of < 0.04 °, which enabled the collection of diffraction from a 2θ range of 20° per scan. Four scans were collected in the range of 20° to 80° 2θ, and radiation was counted for a total duration of 4 h to obtain the XRD profile. The collected data were analyzed using Bruker EVA software. The diffraction data were compared to reference patterns for SnO_2.[1] An FEI Tecnai F30ST transmission-electron microscope with an accelerating voltage of 300 kV was used to image the n-Si/SiO_x/SnO_x interface. A cross section was prepared via mechanical polishing and ion-milling techniques, which limited the TEM analysis to planar Si substrates. Scanning-electron microscope images were collected with a Nova nanoSEM 450 (FEI) instrument on both planar and microcone array photoelectrodes.

Surface Recombination Velocity Measurements

Carrier lifetimes were determined with an instrument and procedure described in previous work.[2] Intrinsically doped 300 μm thick silicon wafers polished in the (111) orientation

with a bulk lifetime > 1.5 ms were chemically oxidized to form a controlled SiO_x layer and coated with 100 SnO_x ALD cycles deposited at 210 °C through the same procedure that was used for n-type silicon wafers. Intrinsically doped Si wafers were utilized for this experiment because the high lifetime of intrinsically doped Si allows the observed recombination to be attributed to surface recombination. Electron-hole pairs were generated in the i-Si/SiO_x/SnO_x sample by a 20 ns, 905 nm laser pulse from an OSRAM diode laser with an ETX-10A-93 driver. A PIN diode connected to an oscilloscope was used to measure the decay in reflected microwave intensity after each excitation. The lifetime was determined by fitting the average decay curve of 64 consecutive scans with an exponential function. The surface recombination velocity was determined from the following relationship:

$$\frac{1}{\tau_m} = \frac{1}{\tau_b} + \frac{2S}{d} \approx \frac{2S}{d}$$

where S is the surface recombination velocity, d is the thickness of the silicon wafer, τ_m is the bulk lifetime, and τ_m is the measured lifetime of the electron-hole pairs.

X-ray Photoelectron Spectroscopy

X-ray photoelectron spectroscopic (XPS) data were collected using a Kratos Axis NOVA (Katros Analytical, Manchester, UK) at a background pressure of < 10^{-9} Torr. A monochromatic Al Kα source at 1486.6 eV was used for excitation. High-resolution scans were collected at a resolution of 0.05 eV and survey scans were collected at 1 eV resolution. All energies including peak energies, valence-band spectra, and work-function measurements were calibrated against the binding energy of the adventitious C 1s peak, which was set at 284.8 eV. For core-level peak energies and valence-band spectra, the bias of the sample was controlled by the XPS instrument,

whereas for work-function measurements the bias of the sample was controlled by an external power supply. Although this study characterized both planar and microcone arrays with photoelectrochemical methods, XPS data were only collected for planar electrodes. The acquired XPS signal has a strong dependence on the angle between the electron emission path and sample surface, so data collection on microcone arrays would result in convolution of the acquired signal with the sample geometry, complicating the quantitative analysis of XPS data.

Using a previously reported procedure, the Ni 2p spectra were fit to determine the composition of the electrodeposited NiFeOOH film.[3] Due to the small projected area coverage of the catalyst on the n-Si/SiO$_x$/SnO$_x$ electrode in conjunction with the overlap of other elemental peaks, the Fe 2p spectra could not be used to quantify the Fe in the electrodeposited film. The Ni 2p$_{3/2}$ spectra of n-Si/SiO$_x$/SnO$_x$/e-NiFeOOH electrodes that had been subjected to 3-5 cyclic voltammetric scans were fit with the reported peak separations, FWHM ratios, and relative peak areas for standard Ni samples. To account for the precision of XPS measurements, the absolute peak positions were allowed to vary within ±0.1 eV of the reported peak position, but the reported peak separations were not adjusted. Only contributions from Ni(OH)$_2$ were required to adequately fit the collected XPS data for the electrodeposited films.

The Co 2p spectra were fit with a previously reported procedure to determine the amount of Co$_3$O$_4$ and Co(OH)$_2$ in the electrodeposited CoO$_x$ film.[4] The Co 2p$_{3/2}$ spectra of n-Si/SiO$_x$/SnO$_x$/CoO$_x$ electrodes operated for 3-5 cyclic voltammetric scans were fit with the reported peak separations, FWHM ratios, and relative peak areas for standard Co samples. To account for the precision of XPS measurements, the absolute peak positions were allowed to vary within ±0.1 eV of the reported peak position, but the reported peak separations were not adjusted. Contributions from both Co$_3$O$_4$ and Co(OH)$_2$ were required to adequately fit the

collected XPS data for the electrodeposited films. The Ir 4f spectra were fit based on the previously reported XP spectra of Ir electrodes for water oxidation in sulfuric acid.[5] Sn 3d spectra could be adequately described by a single component, and this was assigned to SnO_2 based on the previously reported binding energy ranges.[6] Si 2p spectra were fit with previously reported peak shapes.[7] All x-ray photoelectron spectra were processed using CasaXPS. A Shirley background was utilized to correct for the background XPS signal. Most peaks were fit to Gaussian/Lorentzian symmetric line-shapes with a 3:7 Gaussian:Lorentzian contribution unless specified by the literature reference used to assign the XPS peaks.

Electrochemical Testing

The 1.0 M KOH(aq) and 1.0 M H_2SO_4(aq) electrolytes were prepared by dissolving or diluting potassium hydroxide pellets (Sigma-Aldrich, Semiconductor Grade, 99.99%) and sulfuric acid (Fischer Scientific, TraceMetal Grade, 93-98%) with deionized water (18.2 MΩ cm), respectively. The $Fe(CN)_6^{3-/4-}$(aq) electrolyte was prepared by dissolving potassium ferrocyanide trihydrate, potassium ferricyanide, and potassium chloride in deionized H_2O to make a 0.36 M $K_4Fe(CN)_6$/0.05 M $K_3Fe(CN)_6$/0.50 M KCl solution. Digital potentiostats were used to collect the electrochemical data (SP-200 or MPG-2, Bio-Logic Science Instruments). The reference electrodes used in 1.0 M KOH(aq), 1.0 M H_2SO_4(aq), and $Fe(CN)_6^{3-/4-}$(aq) were mercury/mercury oxide (Hg/HgO, CH Instruments), mercury/mercury chloride (SCE, CH Instruments), and a Pt disk (CH instruments), respectively. The Hg/HgO and SCE reference electrodes were calibrated versus a reversible hydrogen electrode (RHE) in 1.0 M KOH(aq) and 1.0 M H_2SO_4(aq), respectively. The RHE consisted of a Pt disk in H_2-saturated electrolyte, with constant bubbling of H_2(g) underneath the Pt disk to ensure H_2 saturation. The calibrated potentials of the Hg/HgO and SCE were 0.906 V and 0. 244 V vs. RHE, respectively. The

counter electrode was a carbon rod in 1.0 M KOH(aq) or 1.0 M H$_2$SO$_4$(aq). Cyclic voltammograms with Pt working, reference, and counter electrodes were used to verify that the Pt equilibrated to the Fe(CN)$_6^{3-/4-}$(aq) Nernstian cell potential. The cyclic voltammograms exhibited zero current at zero voltage versus the Pt reference electrode. The Nernstian potential for Fe(CN)$_6^{3-/4-}$(aq) was 0.31 V vs. SHE based on the concentrations of the redox species. All glassware was cleaned with aqua regia and rinsed with deionized water prior to use. The electrolyte volume was generally ~ 40 mL and cyclic voltammetric data were collected at a scan rate of 40 mV s^{-1}.

Impedance measurements in contact with Fe(CN)$_6^{3-/4-}$(aq) were collected without illumination over a frequency range of 20 Hz to 20 kHz with a sinusoidal wave amplitude of 10 mV. A potential of -0.3 to 0.3 V vs. Fe(CN)$_6^{3-/4-}$ was applied to p$^+$-Si/SiO$_x$/SnO$_x$ electrodes and a potential of 0.0 to 0.6 V vs. Fe(CN)$_6^{3-/4-}$ was applied to n-Si/SiO$_x$/SnO$_x$ electrodes. The impedance measurements were fit with a circuit consisting of a resistor in series with an additional component consisting of a resistor and a capacitor in parallel, as has been described previously.[8] The differential capacitance determined from the impedance measurements on n-Si/SiO$_x$/SnO$_x$ electrodes was attributed to the differential capacitance of the depletion-region of the silicon semiconductor. The differential capacitance determined from the impedance measurements on p$^+$-Si/SiO$_x$/SnO$_x$ electrodes was attributed to the SnO$_x$ layer, due to the voltage dependence suggesting n-type behavior. The potential dependence of the differential capacitance was analyzed using the Mott-Schottky relationship:

$$C_d^{-2} = \frac{2}{qA^2\varepsilon_0\varepsilon_r N_d}\left(V_{app} + V_{bi} - \frac{k_B T}{q}\right)$$

where C_d is the differential capacitance, q is the unsigned charge of an electron, A is the electrode area, ε_0 is the vacuum permittivity, ε_r is the relative permittivity of the semiconductor, N_d is the donor dopant concentration of the semiconductor, V_{app} is the electrode potential vs. $Fe(CN)_6^{3-/4-}$(aq), V_{bi} is the built-in voltage in the semiconductor, and T is the temperature of the electrode while the impedance data were collected. A relative permittivity of $\varepsilon_r = 11.7$ was used to analyze data from n-Si/SiO$_x$/SnO$_x$ electrodes, consistent with previous reports for Si photoanodes. A relative permittivity of $\varepsilon_r = 11.5$ was used to analyze data from p$^+$-Si/SiO$_x$/SnO$_x$ electrodes, corresponding to the average relative permittivity of SnO$_2$.[9] The donor dopant concentration N_d was attributed to the n-Si semiconductor for n-Si/SiO$_x$/SnO$_x$ electrodes, and to SnO$_x$ for p$^+$-Si/SiO$_x$/SnO$_x$ electrodes.

The dissolution of SnO$_x$ deposited with 850 cycles at 210 °C on p$^+$-Si/SiO$_x$ under $\eta = 300$ mV for water oxidation was determined in 1.0 M KOH(aq) and 1.0 M H$_2$SO$_4$(aq). Electrodes with p$^+$-Si instead of n-Si were used to precisely set the surface potential of SnO$_x$. Utilizing an n-Si substrate instead of p$^+$-Si would lead to convolution with the photovoltage generated under illumination, which can vary due to light intensity variability throughout the > 500 h dissolution test. Cells for these experiments had working and reference electrodes separated from the counter electrode by an ion-exchange membrane. An anion-exchange membrane (Fumasep FAA-3-PK-130) and a cation-exchange membrane (Nafion 117) were used for 1.0 M KOH(aq) and 1.0 M H$_2$SO$_4$(aq) electrolytes, respectively. Electrodes with an area of ~ 0.1 cm^2 were held at $\eta = 300$ mV in an initial 50 mL volume of electrolyte. Samples of 200 uL in volume were taken over time and diluted to 5 mL with deionized water. The concentration of Sn was determined using calibration solutions (Semi Metals Plasma Standard Solution, Specpure, Alfa Aesar) and an inductively coupled plasma mass spectrometer (ICP-MS, Agilent 800 Triple Quadrupole). The

concentration of Sn was used to determine the equivalent amount of Sn lost from the electrode, assuming a stoichiometry of SnO_2 and a density equal to the bulk density of SnO_2 (6.95 g cm^{-3}). The amount of Sn removed from the electrolyte during the sample acquisition (200 uL) was taken into account when determining total amount of Sn dissolved from the electrode over time.

Electrochemical Depositions

Nickel-iron oxyhydroxide (NiFeOOH) was electrochemically deposited without illumination at a cathodic current density of -1 mA cm^{-2} on planar electrodes and -10 mA cm^{-2} on microcone arrays. The stirred aqueous solution contained 5×10^{-3} M $Ni(NO_3)_2$ and 5×10^{-3} M $FeSO_4$ in a two-electrode experiment with a single-compartment electrochemical cell that had a carbon rod as a counter electrode. The $Ni(NO_3)_2$(aq) solution was purged with N_2(g) prior to the addition of $FeSO_4 \cdot 6H_2O$(s) to prevent Fe precipitation. Cobalt oxide (CoO_x) was photoelectrochemically deposited from a 0.01 M Co(II) nitrate/0.10 M sodium acetate aqueous solution under 100 mW cm^{-2} of simulated solar illumination with an anodic current density of 1 mA cm^{-2}, using a two-electrode experiment with a single-compartment electrochemical cell with a carbon rod as a counter electrode. The NiFeOOH and CoO_x loadings were controlled by changing the duration of the chronopotentiometric deposition. Iridium oxide (IrO_x) was photoelectrochemically deposited using a modified literature procedure.[10] Aqueous dark-brown solutions of 2×10^{-3} M K_2IrCl_6 and 2×10^{-3} M KOH were heated at 70 °C under continuous stirring until the solution became light-brown and slightly turbid. The solution was then placed in an ice bath to prevent precipitation of Ir species. The electrochemical cell consisted of one compartment with a SCE as a reference electrode and a carbon as a counter electrode. IrO_x was deposited by using cyclic voltammetric scans from -0.2 to 1.2 V vs. SCE under 100 mW cm^{-2} of

simulated solar illumination. The loading of the IrO_x was controlled by changing the number of cyclic voltammetric scans.

Photovoltage Dependence on Surface Area

For junctions that have a constant surface-area-normalized diode current density that is independent of the geometry of the structure, as is expected for well-formed junctions, the observed photovoltage scales with the surface area increase, γ, based on equation 1:[11]

$$V_{oc} = \frac{nk_BT}{q} \ln\left(\frac{J_{ph}}{\gamma J_0}\right)$$

(1)

For the SnO_x heterojunction, the ideality factor was determined to be $n = 1.07$ and the diode current density was $J_0 = 1.3*10^{-11}$ A cm^{-2} for photocurrents between $15 - 60$ mA cm^{-2}. Planar samples exhibited γ = 1, which results in a photovoltage of 596 mV at a photocurrent of 30 mA cm^{-2}, close to that observed in Figure S1a. The n-Si microcone arrays studied herein had a pitch of 7 μm, a height of ~60 μm, and a base diameter of 3.5 μm. The surface area calculated from these dimensions leads to γ ~ 13.3. The photovoltage expected for n-Si microcone array electrodes based on equation 1 is thus 524 mV, for γ = 13.3 at 30 mA cm^{-2} of photocurrent density, which is close to the experimentally observed photovoltage of 490 mV (Figure S9a).
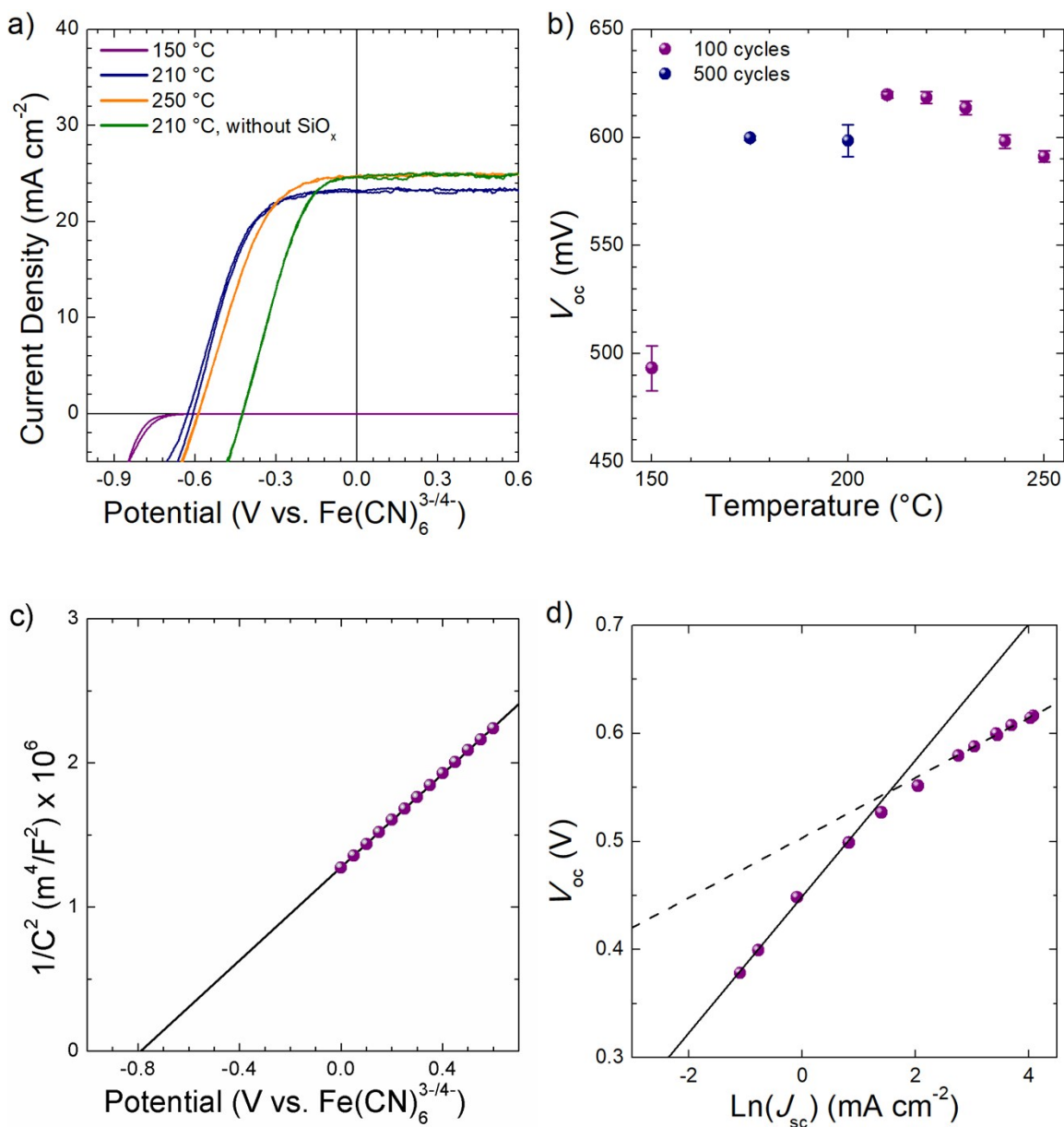
Supplementary Information Figures

Figure S1. Electrochemical behavior of n-Si/SiO$_x$/SnO$_x$ photoanodes coated with SnO$_x$ deposited at temperatures between 150–250 °C in contact with Fe(CN)$_6^{3-/4-}$(aq). a) Photoelectrochemical behavior of n-Si/SiO$_x$/SnO$_x$ photoanodes prepared with 100 SnO$_x$ ALD cycles under 100 mW cm^{-2} of simulated solar illumination, and n-Si/SnO$_x$ photoanodes prepared by depositing SnO$_x$ on HF-etched n-Si substrates. b) Open-circuit voltage of n-Si/SiO$_x$/SnO$_x$

photoanodes prepared with 100 or 500 SnO_x ALD cycles under 100 mW cm^{-2} of simulated solar illumination. c) Mott-Schottky plot of electrode differential capacitance versus voltage of n-$Si/SiO_x/SnO_x$ photoanodes in the dark with a SnO_x layer that was deposited at 210 °C with 100 ALD cycles. d) Open-circuit voltage versus short-circuit current density (V_{oc} vs J_{sc}) plot of -$Si/SiO_x/SnO_x$ deposited at 210 °C in contact with $Fe(CN)_6^{3-/4-}$(aq) under $1 - 200$ mW cm^{-2} of simulated solar illumination.
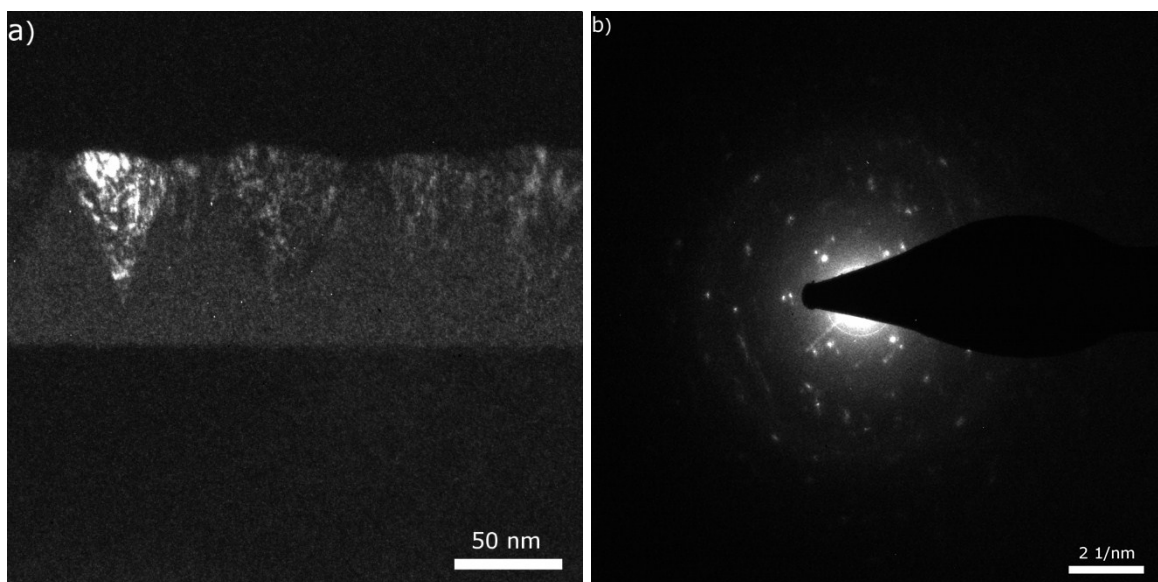
Figure S2. a) Dark field image of n-Si(100)/SiO_x coated with 850 cycles of SnO_x with image brightness corresponding to (002) SnO_2 diffraction signal collected through a 10 μm diemeter aperture. b) Electron diffraction pattern of n-Si/SiO_x coated with 850 cycles of SnO_x, at 300 kV accelerating voltage.
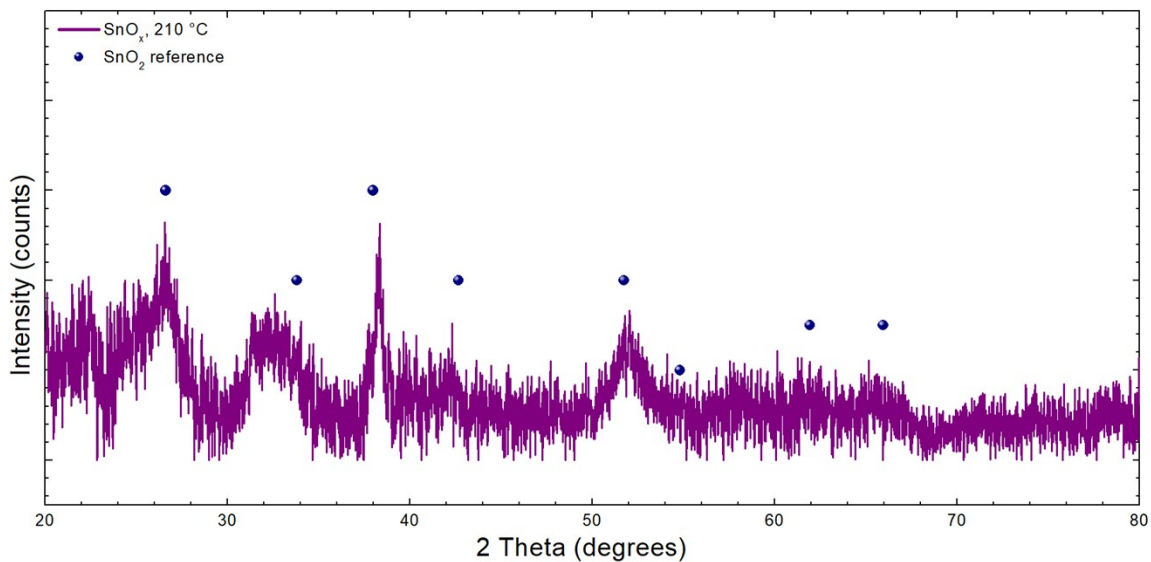
Figure S3. X-ray diffraction pattern for a SnO$_x$ film deposited at 210 °C with 850 ALD cycles on an n-Si(100)/SiO$_x$ substrate. Weak diffraction signals associated with SnO$_2$ were observed.
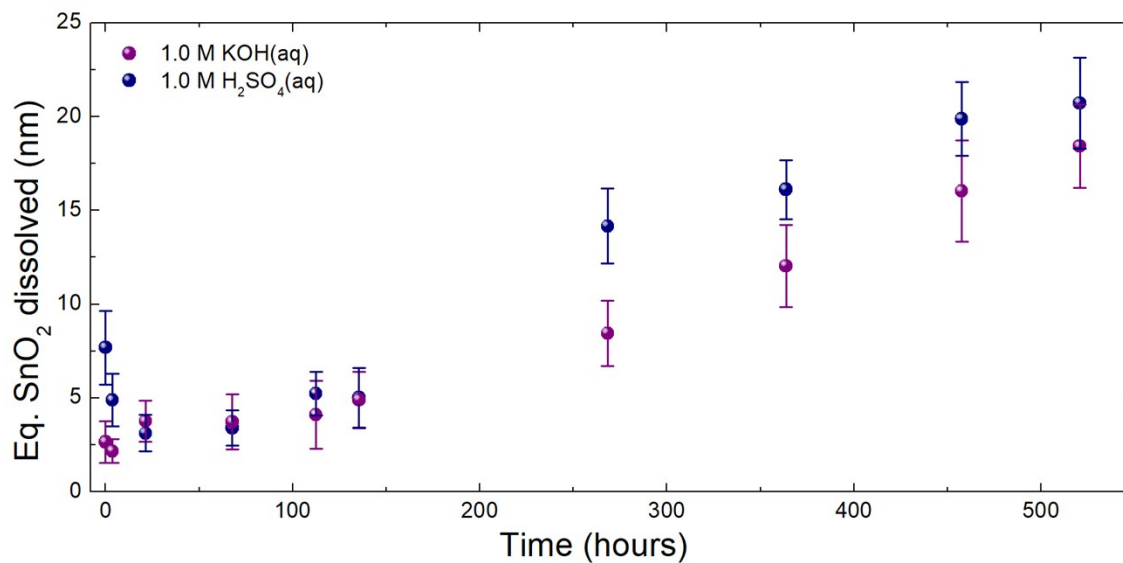

Figure S4. Dissolution of SnO$_x$ film deposited at 210 °C with 850 ALD cycles on a p$^+$-Si(100)/SiO$_x$ substrate. Electrodes were held at 1.53 V vs. RHE in 1.0 M KOH(aq) or 1.0 M H$_2$SO$_4$(aq) eletrolytes.
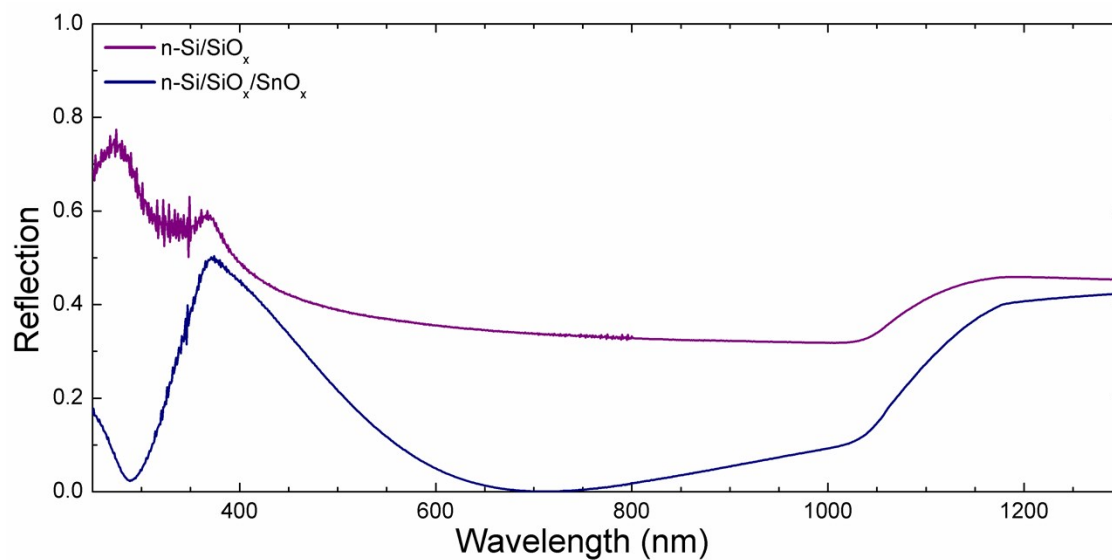
Figure S5. Optical reflectivity measurements at normal incidence of an n-Si/SiO$_x$/SnO$_x$ wafer coated with SnO$_x$ formed at 210 °C with 850 ALD cycles compared to an n-Si wafer with a native silicon oxide layer.
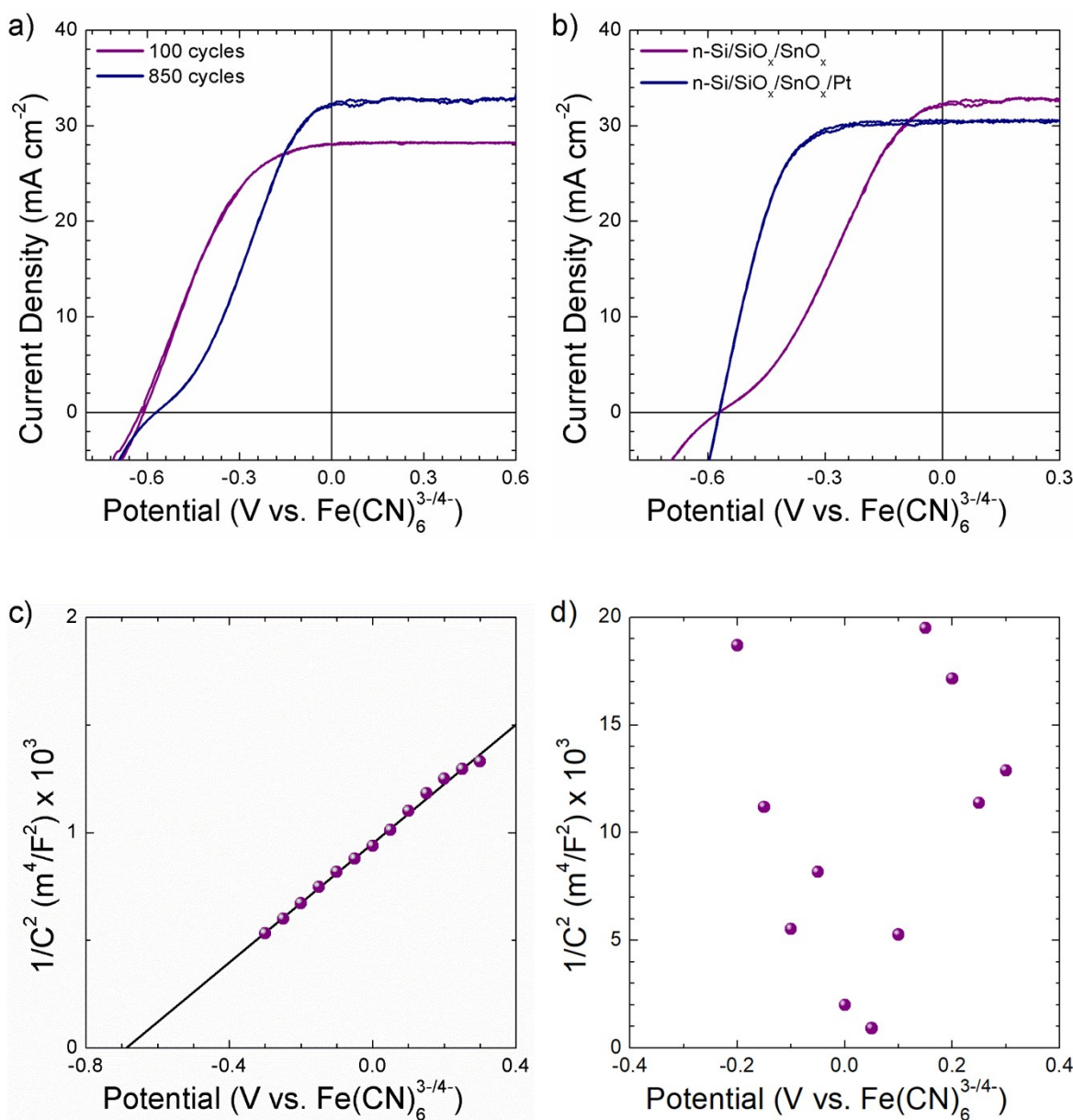
Figure S6. Electrochemical behavior of n-Si/SiO$_x$/SnO$_x$ photoanodes coated with SnO$_x$ deposited at 210 °C in contact with Fe(CN)$_6^{3-/4-}$(aq) under 100 mW cm^{-2} of simulated solar illumination. a) Photoelectrochemical behavior of n-Si/SiO$_x$/SnO$_x$ photoanodes with 100 or 850 ALD SnO$_x$ cycles. b) Photoelectrochemical behavior of n-Si/SiO$_x$ photoanodes with 850 cycles of SnO$_x$ with and without a sputtered Pt overlayer. c) Mott-Schottky plot of electrode differential apacitance versus potential of p$^+$-Si/SiO$_x$/SnO$_x$ electrodes in the dark with a SnO$_x$ layer deposited

at 210 °C with 850 ALD cycles. d) Mott-Schottky plot of electrode differential capacitance versus potential for p^+-Si/SiO$_x$/SnO$_x$/Pt in the dark, indicating no apparent band bending.
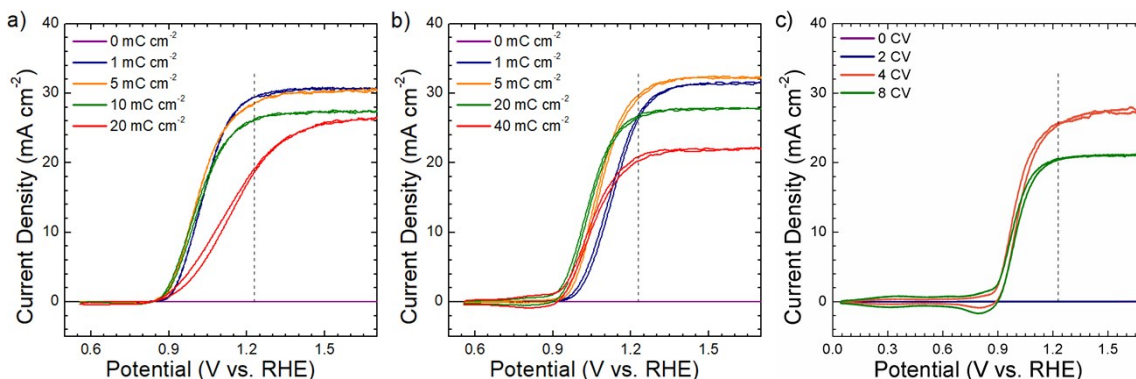

Figure S7. Photoelectrochemical behavior of planar n-Si/SiO$_x$ photoanodes coated with 100 cycles of SnO$_x$ and electrodeposited water oxidation catalysts in contact with 1.0 M KOH(aq) under 100 mW cm^{-2} of simulated solar illumination. a) Photoanodes with different amounts of NiFeOOH electrodeposited in the dark at a current density of 1 mA cm^{-2}. b) Photoanodes with different amounts of CoO$_x$ photoelectrodeposited under 100 mW cm^{-2} of simulated solar illumination at a photocurrent density of 1 mA cm^{-2}. c) Photoanodes with different amounts of IrO$_x$ photoelectrodeposited under 100 mW cm^{-2} of simulated solar illumination with a cyclic voltammetry procedure.
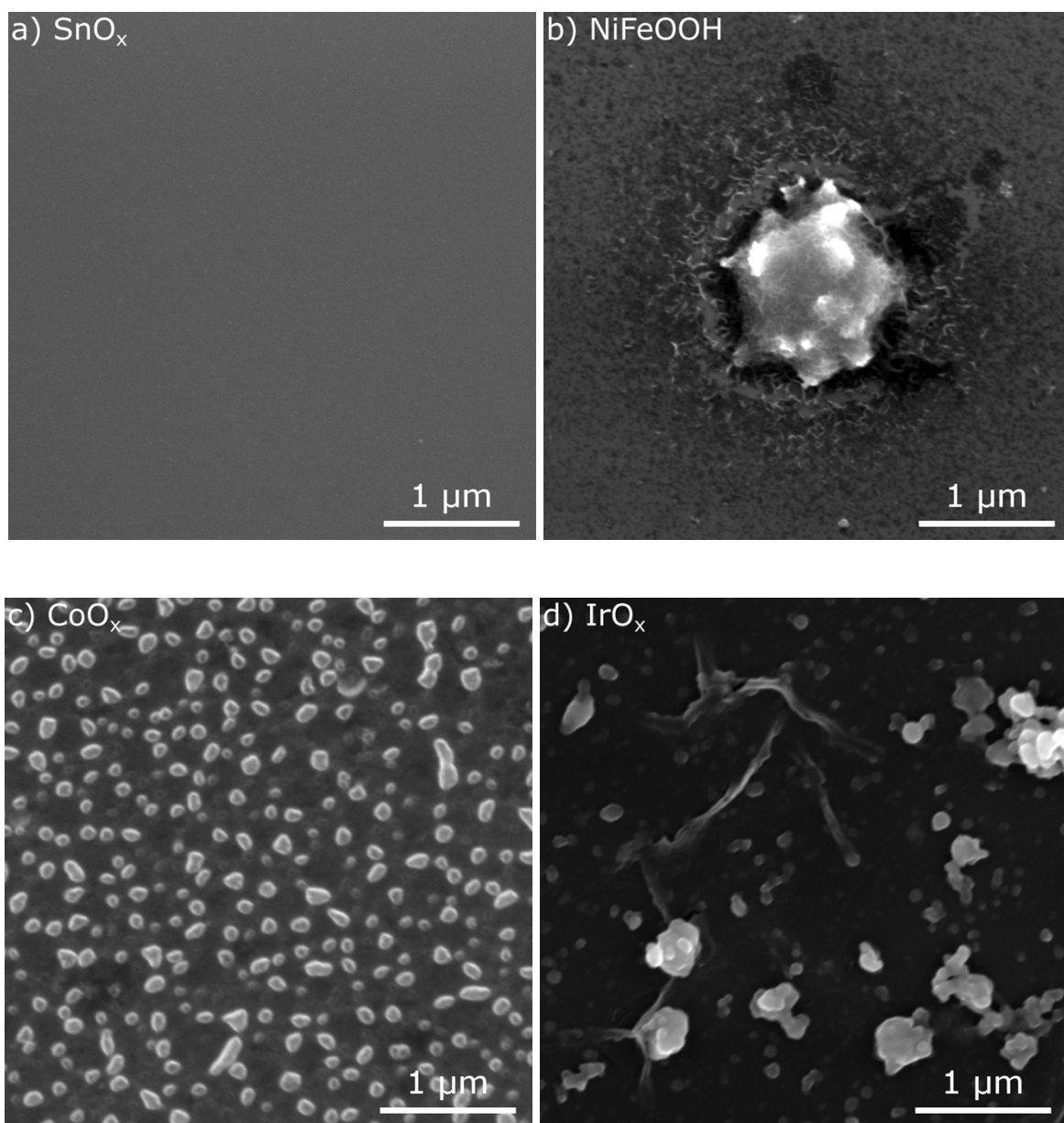
Figure S8. Scanning-electron miscroscopy images of n-Si/SiO$_x$ photoanodes with 100 cycles of SnO$_x$ and various electrodeposited water-oxidation catalysts. a) Bare SnO$_x$ surface. b) SnO$_x$ with electrodeposited 5 mC cm^{-2} of electrodeposited NiFeOOH. c) SnO$_x$ with 5 mC cm^{-2} of electrodeposited CoO$_x$. d) SnO$_x$ with IrO$_x$ deposited with 4 cyclic voltammetric scans.
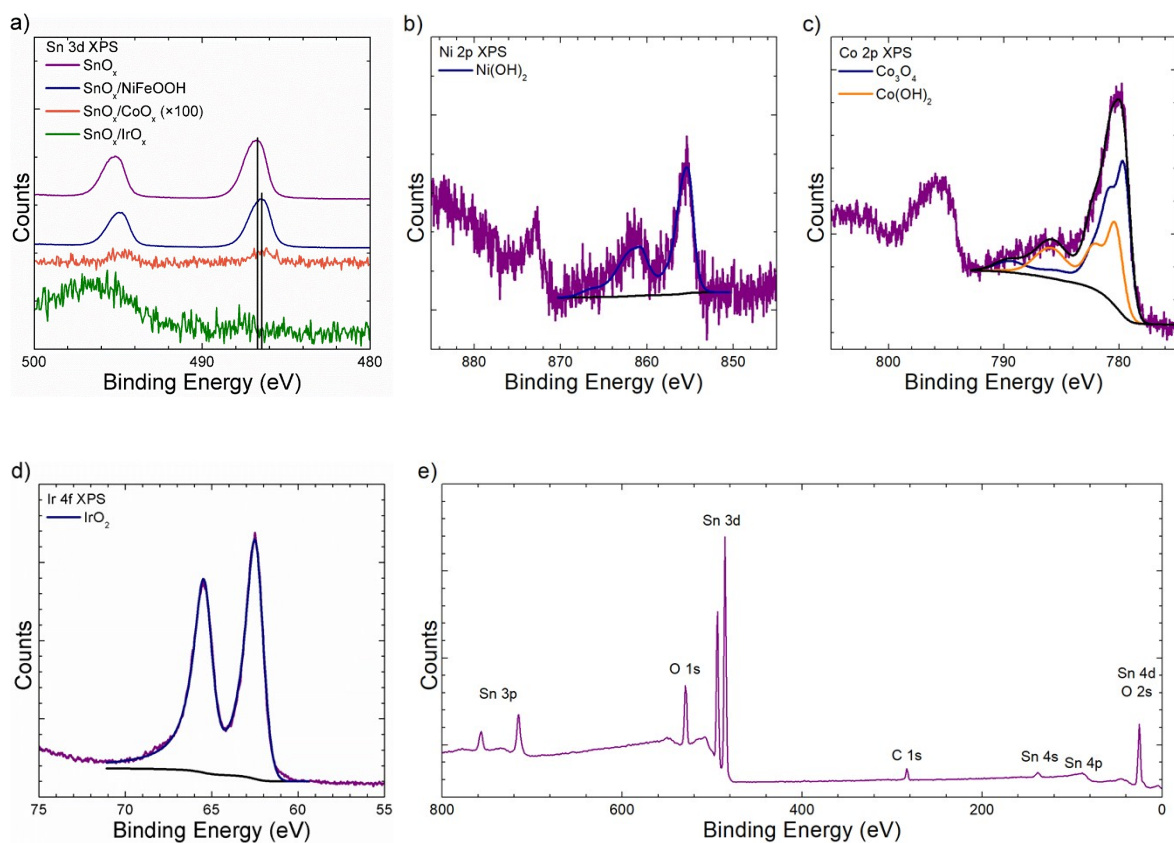
Figure S9. High-resolution XPS data of n-Si/SiO$_x$ photoanodes with 100 cycles of SnO$_x$ and various electrodeposited water oxidation catalysts after 3-5 cyclic voltammetric scans. a) Sn 3d spectra b) Ni 2p spectra. c) Co 2p spectra. d) Ir 4f spectra. e) Survey scan of SnO$_x$ film indicating the presence of Sn, O, and adventitious C.
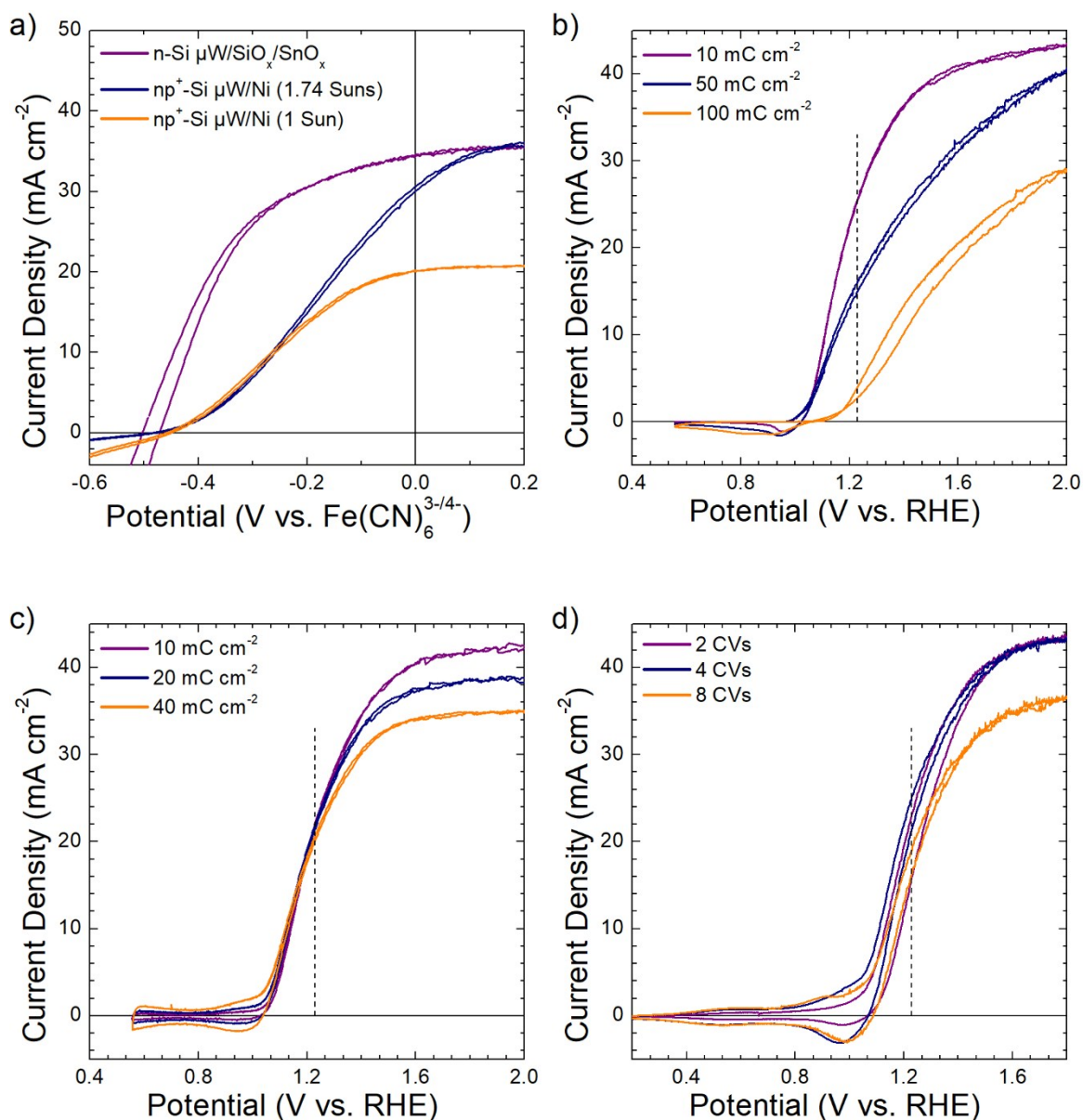
Figure S10. a) Photoelectrochemical behavior of n-Si microcone array/SiO$_x$ coated with 100 cycles of SnO$_x$ in contact with Fe(CN)$_6^{3-/4-}$(aq) under 100 mW cm^{-2} of simulated solar illumination and np$^+$-Si microcone array/Ni electrodes under 100 mW cm^{-2} of illumination, as well as under 174 mW cm^{-2} of illumination to obtain a photocurrent density similar to n-Si microcone array/SiO$_x$/SnO$_x$ devices. b) Photoelectrochemical behavior under water oxidation conditions in 1.0 M KOH(aq) of n-Si microcone array/SiO$_x$/SnO$_x$ electrodes with different

amounts of cathodically deposited NiFeOOH. c) Photoelectrochemical behavior in 1.0 M KOH(aq) of n-Si microcone array/SiO_x/SnO_x electrodes with different amounts of anodically deposited CoO_x. d) Photoelectrochemical behavior in 1.0 M H_2SO_4(aq) of n-Si microcone array/SiO_x/SnO_x electrodes with different amounts of anodically deposited IrO_x.
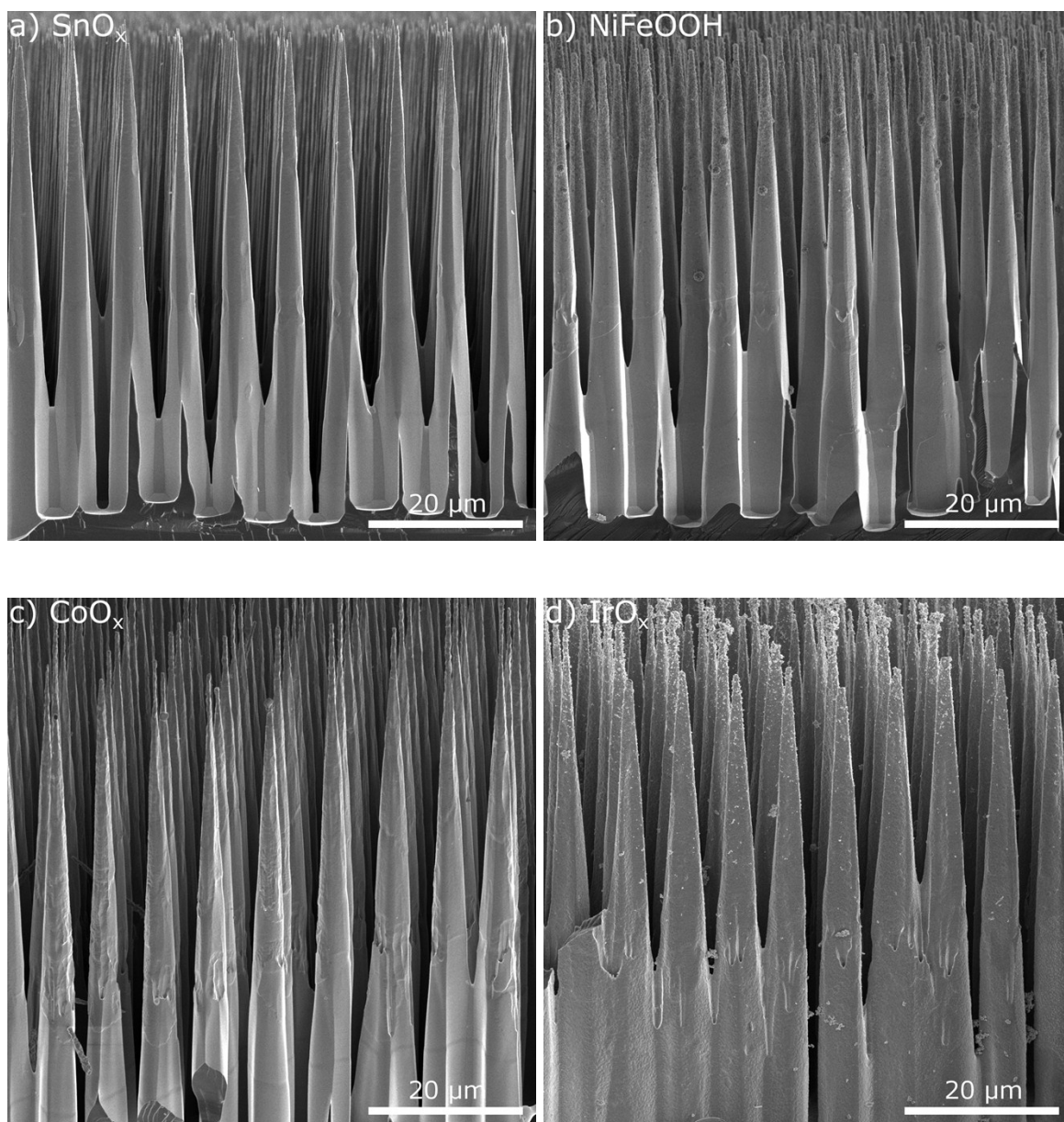

Figure S11. Scanning-electron miscroscopy images of n-Si microcone array/SiO_x electrodes coated with 100 cycles of SnO_x and various (photo)electrodeposited catalysts. a) n-Si microcones

prior to (photo)electrodeposition of catalysts, b) n-Si microcones with NiFeOOH electrochemically deposited with 10 mC cm^{-2}, c) n-Si microcones with CoO$_x$ photoelectrochemically deposited with 10 mC cm^{-2}, d) n-Si microcones with IrO$_x$ photoelectrochemically deposited with 2 cyclic voltammograms.
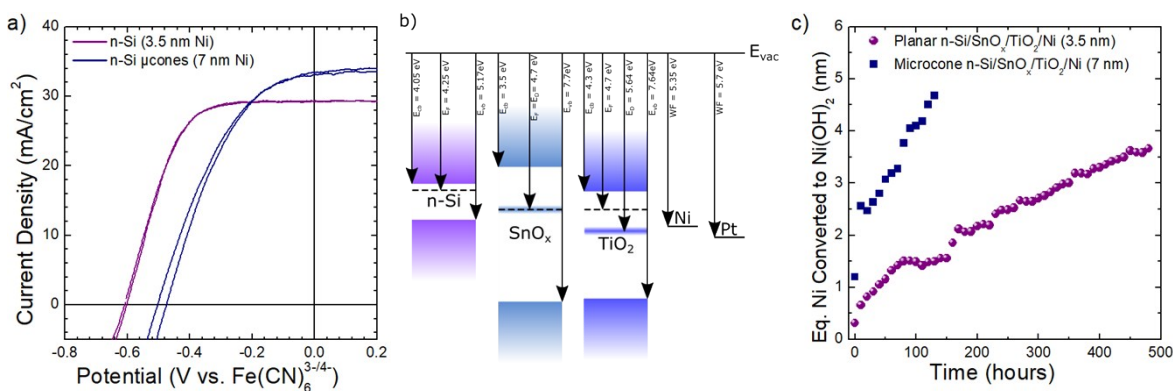

Figure S12. a) Photoelectrochemical behavior of n-Si/SiO$_x$ and n-Si microcone array/SiO$_x$ photoanodes coated with 400 cycles of SnO$_x$, 900 cycles of TiO$_2$, and sputter-deposited Ni in contact with Fe(CN)$_6^{3-/4-}$(aq) under 100 mW cm^{-2} of simulated solar illumination. b) Band energetics of n-Si, SnO$_x$, TiO$_2$, Ni, and Pt with respect to the vaccum energy. The band energetics of TiO$_2$, Ni, and Pt were obtained from previous reports.[7, 12] c) Conversion of Ni to Ni(OH)$_2$/NiOOH on planar and microcone array n-Si/SiO$_x$/SnO$_x$/TiO$_2$/Ni electrodes during operation in 1.0 M KOH under 100 mW cm^{-2} of simulated solar illumination. The amount of Ni converted was determined by integrating the cathodic peak from the Ni(OH)$_2$/NiOOH redox couple and using the conversion factor of 1.46 mC cm^{-2} of cathodic charge per nm of Ni.

Table S1. Photoelectrochemical behaviour of n-Si photoelectrodes under 100 mW cm^{-2} of simulated solar illumination.

n-Si(100)/SiO$_x$ Photoelectrode Coating	Electrolyte [1.0 M]	Overpotential at 1 mA cm^{-2} [mV]	Photocurrent Density [mA cm^{-2}]	Solar-to-O$_2$(g) Efficiency [%]
SnO$_x$/NiFeOOH	KOH	-339	30.1	3.5
SnO$_x$/CoO$_x$	KOH	-287	32.2	2.6
SnO$_x$/IrO$_x$	H$_2$SO$_4$	-384	27.1	3.1
SnO$_x$/TiO$_2$/Ni	KOH	-301	28.3	3.5

n-Si(μcn)/SiO$_x$ Photoelectrode Coating	Electrolyte [1.0 M]	Overpotential at 1 mA cm^{-2} [mV]	Photocurrent Density [mA cm^{-2}]	Solar-to-O$_2$(g) Efficiency [%]
SnO$_x$/NiFeOOH	KOH	-186	41.2	1.3
SnO$_x$/CoO$_x$	KOH	-167	41.0	0.9
SnO$_x$/IrO$_x$	H$_2$SO$_4$	-147	42.1	1.0
SnO$_x$/TiO$_2$/Ni	KOH	-148	30.2	0.5

References

1.   W. H. Baur and A. A. Khan, *Acta Cryst.*, 1971, **B27**, 2133-2139.

2.   N. T. Plymale, Y.-G. Kim, M. P. Soriaga, B. S. Brunschwig and N. S. Lewis, *J. Phys. Chem. C*, 2015, **119**, 19847-19862.

3.   M. C. Biesinger, B. P. Payne, L. W. M. Lau, A. Gerson and R. S. C. Smart, *Surf. Interface Anal.*, 2009, **41**, 324-332.

4.   M. C. Biesinger, B. P. Payne, A. P. Grosvenor, L. W. M. Lau, A. R. Gerson and R. S. C. Smart, *Appl. Surf. Sci.*, 2011, **257**, 2717-2730.

5.   H. Y. Hall and P. M. A. Sherwood, *J. Chem. Soc., Faraday Trans. 1*, 1984, **80**, 135-152.

6.   J. M. Themlin, M. Chtaib, L. Henrard, P. Lambin, J. Darville and J. M. Gilles, *Phys. Rev. B*, 1992, **46**, 2460-2466.

7.   S. Hu, M. H. Richter, M. F. Lichterman, J. Beardslee, T. Mayer, B. S. Brunschwig and N. S. Lewis, *J. Phys. Chem. C*, 2016, **120**, 3117-3129.

8.   X. Zhou, R. Liu, K. Sun, K. M. Papadantonakis, B. S. Brunschwig and N. S. Lewis, *Energy Environ. Sci.*, 2016, DOI: 10.1039/c5ee03655k.

9.   H. J. van Daal, *J. Appl. Phys.*, 1968, **39**, 4467-4469.

10.   Y. Zhao, N. M. Vargas-Barbosa, E. A. Hernandez-Pagan and T. E. Mallouk, *Small*, 2011, **7**, 2087-2093.

11.   E. L. Warren, H. A. Atwater and N. S. Lewis, *J. Phys. Chem. C*, 2013, **118**, 747-759.

12.   H. L. Skriver and N. M. Rosengaard, *Phys. Rev. B*, 1992, **46**, 7157-7168.